JACS
JOURNAL OF THE AMERICAN CHEMICAL SOCIETY
Communication
pubs.acs.org/JACS

Enrichment and Encapsulation of Uranium with Iron Nanoparticle

Lan Ling and Wei-xian Zhang*

State Key Laboratory for Pollution Control and Resource Reuse, College of Environmental Science and Engineering, Tongji University, Shanghai, China

Supporting Information

ABSTRACT: The ability to recover uranium from water is significant because of its potential applications on nuclear fuel capture and mitigation of nuclear wastes. In this work, a unique nanostructure is presented by which trace level (2.32−882.68 μg/L) uranium can be quickly separated from water and encapsulated at the center of zero-valent iron nanoparticles. Over 90% of the uranium is recovered with 1 g/L nanoparticles in less than 2 min. Near atomic-resolution elemental mapping on the U(VI) intraparticle reactions in a single iron nanoparticle is obtained with aberration corrected scanning transmission electron microscopy, which provides direct evidence on U(VI) diffusion, reduction to U(IV), and deposition in the core area.

Separation of trace level uranium from water has long been a technological challenge for two imperative reasons: the growing demand for nuclear fuel and the complexity of nuclear waste management.[1−3] For example, there is a growing demand for nonfossil energy in China, which is fully exampled by the 30 nuclear reactor units with a total capacity of 29 240 MW currently under construction.[4,5] Given limited geological deposits of nuclear fuels, scientists have long been searching unconventional sources for uranium. The largest source of uranium is seawater, which contains, on the average, 3.3 ppb of uranium and has a total uranium reserve estimated at 4.5 billion tons.[6−8] Meanwhile, nuclear waste management also persists as one of society's most physically taxing issues.[9−11] An increasing amount of radioactive wastes has been accumulated by power plants, hospitals, and research facilities, as well as from the legacy nuclear weapons programs of the Cold War era. After the 2011 Fukushima nuclear disaster, facilities utilized to decontaminate the alarming amount of radioactive wastewater from the damaged reactors repeatedly failed.[12,13] These developments clearly exposed the vulnerability and limitations of current radioactive waste treatment and management technologies.

In this work, instant separation, enrichment, and encapsulation of low-level uranium from water is demonstrated with nanoscale zero-valent iron (nZVI), which is increasingly being used in hazardous waste treatment and environmental remediation,[14−16] and has been suggested as a potential agent for uranium immobilization.[17−22]

As shown in Figure 1, rapid and near complete removal of uranium from water was achieved in batch experiments with uranium concentrations in the range of 2.32−882.68 μg/L. In all experiments, the residual uranium concentration in water was reduced below 1 μg/L within 2 min under completely mixed conditions (Figure 1; more information is provided in the Figure S1). The uranium solution was prepared with deionized water plus 0.46 M NaCl, 0.20 M $MgCl_2$, 0.03 M $MgSO_4$ and 0.01 M $CaCl_2$ to simulate the effect of salinity. Samples were filtered for the measurements of dissolved uranium concentration. Total dissolved uranium was measured by the method of inductively coupled plasma mass spectrometry (ICP−MS). More details on the methods and materials are provided in the Supporting Information. The solution containing nZVI was highly reducing with standard potential (Eh) below −500 mV. Experiments with solution pH from 3.5 to 8 found no apparent pH impact on the separation efficiency and rate. Tests were also done with repeated dosing of the nZVI solution with uranium at 50−300 mg/L. Contents of uranium in the reacted iron nanoparticles were measured in the range of 0.24 to 1.41 g of U/g of Fe.

Various mechanisms on the U−Fe reactions have been proposed including the direct reduction of U(VI) by both ferrous iron [Fe(II)] and metallic iron [Fe^0] to form the less soluble U(IV) products (e.g., UO_2), sorption onto iron oxides, and/or combinations of reduction/precipitation/sorption.[21,22] Nonetheless, direct evidence on the key intraparticle reaction steps is still scarce.

In this work, fundamental questions of uranium enrichment and U(VI)-Fe^0 reactions including the diffusion and reaction processes in the nanoparticles were studied with aberration corrected scanning transmission electron microscopy (Cs-STEM) integrated with X-ray energy dispersive spectroscopy (XEDS), electron energy-loss spectroscopy (EELS), and X-ray photoelectron spectroscopy (XPS), which provide accurate and simultaneous near-atomic resolution visualization on the U(VI) diffusion and reactions within a single nanoparticle.[23−26]

The nZVI nanoparticles are spherical in shape with sizes ranging from 20 to 100 nm and often present as chain-like aggregates due to magnetic attractions, colloidal aggregation, and the formation of a continuous layer of iron hydroxide on the surface (Figure S2).[17,23,24,27] Individual nanoparticles comprise a metallic iron core and separate from each other by a thin (∼2−4 nm) interfacial iron oxide layer. The secondary electron images (Figure S2d), which are obtained with a Hitachi HD-2700 STEM, give rich depth information about the surface and offer three-dimensional characteristics of the spherical nZVI particles. HAADF images show that regions of the specimen with greater atomic number appear brighter, that is, the particle consists of a bright core, corresponding to

Received: October 12, 2014
Published: February 17, 2015

ACS Publications © 2015 American Chemical Society

DOI: 10.1021/ja510488r
J. Am. Chem. Soc. 2015, 137, 2788−2791

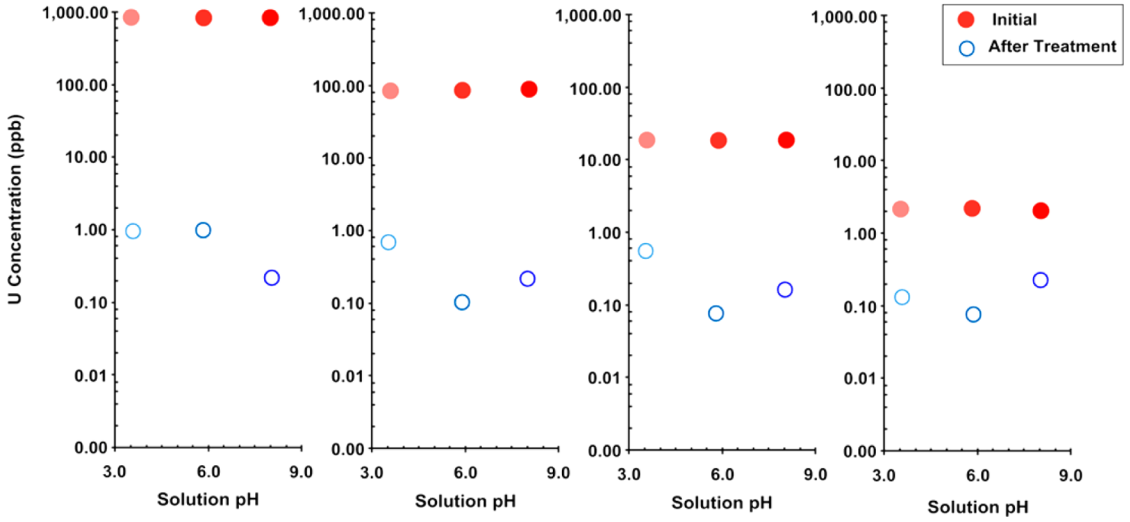

Figure 1. Separation of uranyl nitrate from water with nanoscale zero-valent iron (nZVI). Initial uranyl nitrate $[UO_2(NO_3)_2{\cdot}6H_2O]$ concentrations were in the range of 0.0097 to 3.71 μmol (2.32 to 882.68 μg/L as U) as indicated in the figure. nZVI concentration was 1.0 g/L. The solid red circles represent the initial concentrations of uranium in water, while the empty blue ones symbol those after 1 h reactions.

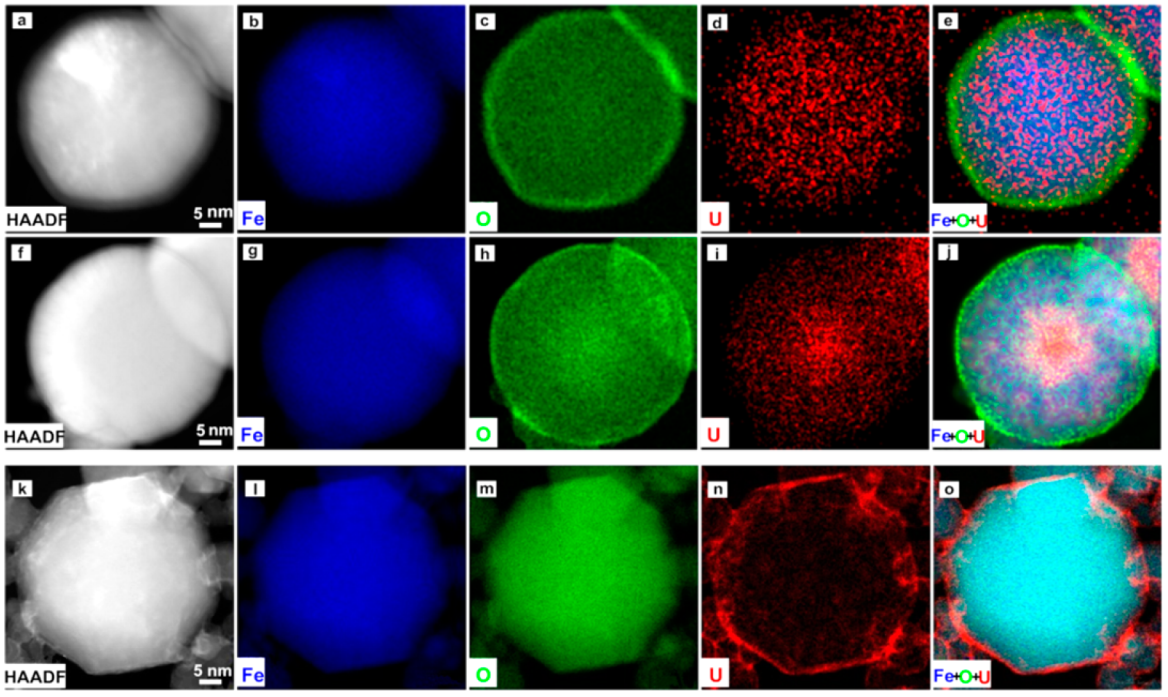

Figure 2. STEM XEDS mappings of uranium reactions with hematite (Fe_2O_3) and nZVI: (a–e) after 1 h with nZVI; (f–j) after 24 h with nZVI; (k–o) after 24 h with hematite. (a,f,k) HAADF images; (b,g,l) Fe mapping; (c,h,m) O mapping; (d,i,n) U mapping; (e,j,o) Fe + O + U color overlays.

the metallic iron, while the outer layer appears dim due to the presence of lower atomic weight oxygen atoms. The core–shell configuration bestows the nanoparticles the reductive character of metallic iron as well as adsorptive and coordinative properties of iron oxides in water. In a HAADF image, uranium appears much brighter due to its large atomic mass.[23−25] After reactions with U(VI), the spherical shape of nZVI nanoparticles was degraded to form irregular grain boundaries and bumpy surfaces (Figure S3), while the spent nZVI still preserved the core–shell structure with a bright core and a lower intensity shell (Figure S3f).

Figure 2 presents the STEM-XEDS elemental mapping of Fe(Kα), U(Lα), and O(Kα) and corresponding color overlays of one nZVI particle. Additional tests were also done with a sample of nanoscale iron oxide (hematite, Fe_2O_3) as a benchmark material to contrast the surface sorption of uranium. The mappings obtain the abundance of iron, oxygen, and uranium in a single nanoparticle and, more importantly, illustrate distinctive patterns of uranium distributions in the nanoparticle (more mappings from different particles are provided in Figure S4). For the nZVI particle after 1 h reactions (Figure 2a–e), the Fe scan (Figure 2b) indicates steep decrease in the iron signal intensity and hence significant loss of iron near the surface. The oxygen distribution (Figure 2c) demonstrates wide-ranging presence, particularly showing a dense surface ring. The uranium mapping illustrates that the outline of uranium area (Figure 2d,e) is slightly smaller than those of iron (Figure 2b) and oxygen (Figure 2c), thus

DOI: 10.1021/ja510488r
J. Am. Chem. Soc. 2015, 137, 2788–2791

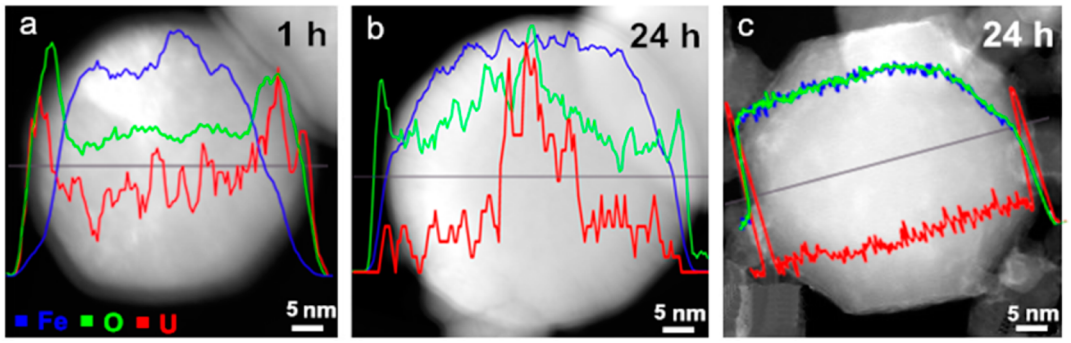

Figure 3. Representative STEM-XEDS line profiles of uranium in (a) nZVI after 1 h; (b) nZVI after 24 h; (c) uranium in iron oxide (hematite, Fe_2O_3) after 24 h. nZVI/Fe_2O_3 = 1.0 g/L; $UO_2(NO_3)_2$ = 100 mg/L as U.

suggesting that uranium has penetrated the surface oxide layer. However, uranium after 1 h exhibits wide-range spreading and dispersion inside the nanoparticle (Figure 2d,e) and, subsequently, is highly concentrated near the particle center to form a nucleus-like structure after 24 h (Figure 2i,j). For the iron oxide, the particle looks like a near-perfect octagon with brighter and somewhat uneven surface coating, particularly on the edges after reactions. Areas of Fe and O also present nicely as octagon-like arrangements with the uranium populated on the exterior surface (Figure 2k–o).

Amusing information on the intraparticle distribution and mass transfer of uranium during the reactions is also acquired with the STEM-XEDS line profiles (Figure 3). After 1 h reactions with nZVI, uranium clearly diffuses through the iron oxide shell with the uranium peak located inside the shell and near the iron oxide–Fe^0 interface (Figure 3a). Subsequently, the uranium peak diffuses inward and establishes at the particle center after 24 h (Figure 3b). Meanwhile, the area of oxygen is much more extensive than that of the spent nZVI for 1 h reactions, with both U and O entrenched deeper inside the particle. The elemental line profiles on the spent Fe_2O_3 reconfirms that the uranium is just attached to the surface with peaks located right on the outer surface (Figure 3c).

XEDS quantification analysis further demonstrates the power of nZVI for uranium sequestration and enrichment: 38% of the total uranium deposited near the center (10% of volume) of the nZVI particle after 24 h, while the central 50% volume contained approximately 87.3% of the uranium in the solid phase. In comparison, uranium after 1 h is mostly (>80%) on the outer shell (~25% volume) of nZVI, and all uranium associated with the iron oxide is deposited on the surface and within fractures (Figure 3c).

In addition to the uranium translocation and distribution, chemical reactions in nanoparticles, i.e., the reduction of U(VI) to U(IV) is confirmed with two independent methods: EELS and XPS (data are provided in Figures S4 and S5). From the EELS $O_{4,5}$ (5d → 5f) edges of uranium (Figure S5), spectra of U on hematite and on the nZVI surface contained a small peak at low energy (prepeak, at ~96 eV) and a large peak at ~111 eV. According to previous studies,[28,29] the large peak (~111 eV) encapsulates both the O_4 ($5d_{3/2}$) and O_5 ($5d_{5/2}$) given by the transitions of U(IV) $5d^{10}5f^06d^07s^0$ to $5d^95f^16d^07s^0$. In short, those two peaks confirm the accumulation of U(VI) on hematite and also on the nZVI surface.[28,29] In contrast, the existence of U(IV) in the nZVI core area is corroborated by the spectra of uranium with two big resonances (the bottom curve of Figure S5). A new shoulder emerges on the high energy side of the larger peak (~111 eV) resulting from two electrons in the 5f states of the U(IV) electron configuration ($5f^26d^07s^0$). XPS characterization provides independent proof that U(VI) is indeed reduced to U(IV) (Figure S6). Meanwhile, XPS sputtering analysis corroborates the presence of uranium in the surface layer with even more in the interior.

The observed patterns of uranium diffusion and reduction within nZVI can be fully interpreted based on the structure of nZVI, which contains two nanoscale components (the metallic iron and oxides). The surface iron oxide/hydroxide layer offers the reactive (polar and charged) sites for the initial attraction and coordinative sorption of UO_2^{2+}. The mass transfer of uranium from bulk solution to the center of nZVI entails many steps. Sorption or attachment step is reversible depending on solution pH and very fast due to the small size and large surface area of nZVI and the mixed valence iron oxide shell.[23] Further penetration or diffusion across the oxide layer is accelerated by its chemical reduction mediated by ferrous and/or Fe^0. Previous work also shows that defects on the particle surface offer potential breakthrough conduits for the uranium to "attack" the core area, which is filled with Fe^0, the electron donor for U(VI) reduction.[23,24] Ultimately, the most favored destination for the uranium reduction and immobilization is at the particle center where the concentration of Fe^0 is the highest. Accordingly, U(VI) is rapidly reduced and embedded in the nanostructure instead of being retained merely as reversible surface-bound species.

nZVI has exhibited much larger uranium removal capacity than conventional metal oxides and polymeric sorbents, which have been the choice of materials for uranium extraction from water so far.[18−22] Batch experiments with repeated spikes of concentrated (up to 300 mg of U/L) uranyl confirmed that the observed removal capacity was as high as 2.4 g of U/g of Fe. This is consistent with our previous work on the removal of oxyanions such As(V), Se(VI), and Cr(VI), with very large capacity (≥1 g/g Fe) for the separation of oxyanions.[23,24] The extensive oxidation of nZVI and accumulation of uranium in the particle center underline the very favorable stoichiometry of nZVI for uranium reduction and sequestration ($3UO_2^{2+}$:$2Fe^0$). Theoretically, 1 mol of Fe can reduce 1.5 mol of U(VI), that is, 1 g of iron has ample electrons to reduce 6.4 g of uranium. Because of the large differentiation in the standard potential (Eh^0), there exists a large driving force for fast U(VI) reduction by the zero-valent iron. This is the fundamental reason that nZVI is more effective than conventional sorbents. Materials based on sorption alone tend to have relatively low capacity and fast release of uranium upon even modest changes in the solution pH.

DOI: 10.1021/ja510488r
J. Am. Chem. Soc. 2015, 137, 2788−2791

The reduced uranium is also stable in the presence of zero-valent iron. This offers a crucial advantage for nuclear waste containment and management. The captured uranium can be further stabilized with the conversion of surface iron oxides back to Fe^0 via chemical reduction and reinforced with a surface coating of heavy metals such as lead. Last but not the least, a key benefit of nZVI is the easy separation of the uranium-laden iron nanoparticles from water. The nanosized iron particles can be effectively retrieved from water with a common magnet (as illustrated in Figure S8), such that the iron nanoparticles can be separated, recycled, and reused at high efficiency. This can vastly increase the uranium loading in the iron nanoparticles and reduce the cost. In short, the fast reactions, large capacity, easy separation, and stable chemical structures make nZVI a promising agent for the enrichment, isolation, and stabilization of trace-level uranium from water.

■ ASSOCIATED CONTENT

Supporting Information

Figures S1−S9 and experimental details. This material is available free of charge via the Internet at http://pubs.acs.org.

■ AUTHOR INFORMATION

Corresponding Author

*zhangwx@tongji.edu.cn

Notes

The authors declare no competing financial interest.

■ ACKNOWLEDGMENTS

Financial support from the National Natural Science Foundation of China (NSFC Grants 21277102 and 21307094), the Science and Technology Commission of Shanghai (Grant 11JC1412600), and the Collaborative Innovation Center for Regional Environmental Quality are acknowledged. Technical support from Drs. Anna Carlsson and Liang Zhang of FEI on the use of FEI Titan S/TEM is greatly appreciated.

■ REFERENCES

(1) Schneider, M.; Froggatt, A. *Bull. At. Sci.* **2014**, *70*, 70−84.
(2) Ahearne, J. F. *Energy Econ.* **2011**, *33*, 572−580.
(3) Saito, S. *J. Nucl. Mater.* **2010**, *398*, 1−9.
(4) Zhou, S.; Zhang, X. L. *Energy* **2010**, *35*, 4282−4288.
(5) Yuan, J. H.; Xu, Y.; Kang, J. J.; Zhang, X. P.; Hu, Z. *Energy* **2014**, *67*, 27−40.
(6) Davies, R. V.; Kennedy, J.; Mcilroy, R. W.; Spence, R.; Hill, K. M. *Nature* **1964**, *203*, 1110−1115.
(7) Sather, A. C.; Berryman, O. B., Jr.; Rebek, J. *J. Am. Chem. Soc.* **2010**, *132*, 13572−13574.
(8) Manolis, J. M.; Mercouri, G. K. *J. Am. Chem. Soc.* **2012**, *134*, 16441−16446.
(9) Priest, N. D. *Lancet* **2001**, *357*, 244−249.
(10) Craft, E. S.; Abu-Qare, A. W.; Flaherty, M. M.; Garofolo, M. C.; Rincavage, H. L.; Abou-Donia, M. B. *J. Toxicol. Environ. Health B* **2004**, *7*, 297−317.
(11) Yasunari, T. J.; Stohl, A.; Hayano, R. S.; Burkhart, J. F.; Eckhardt, S.; Yasunari, T. *Proc. Natl. Acad. Sci. U.S.A.* **2011**, *108*, 19530−19534.
(12) Buesseler, K.; Aoyama, M.; Fukasawa, M. *Environ. Sci. Technol.* **2011**, *45*, 9931−9935.
(13) Kinoshita, N.; Sueki, K.; Sasa, K.; Kitagawa, J.; Ikarashi, S.; Nishimura, T.; Wong, Y. S.; Satou, Y.; Handa, K.; Takahashi, T. *Proc. Natl. Acad. Sci. U.S.A.* **2011**, *108*, 19526−19529.
(14) Wang, C. B.; Zhang, W. X. *Environ. Sci. Technol.* **1997**, *31*, 2154−2156.
(15) Ponder, S. M.; Darab, J. G.; Mallouk, T. E. *Environ. Sci. Technol.* **2000**, *34*, 2564−2569.
(16) Matheson, L. J.; Tratnyek, P. G. *Environ. Sci. Technol.* **1994**, *28*, 2045−2053.
(17) Zhang, W. X. *J. Nanopart. Res.* **2003**, *5*, 323−332.
(18) Morrison, S. J.; Metzler, D. R.; Carpenter, C. E. *Environ. Sci. Technol.* **2001**, *35*, 385−390.
(19) Gu, B.; Liang, L.; Dickey, M. J.; Yin, X.; Dai, S. *Environ. Sci. Technol.* **1998**, *32*, 3366−3373.
(20) Yan, S.; Hua, B.; Bao, Z. Y.; Yang, J.; Liu, C. X.; Deng, B. L. *Environ. Sci. Technol.* **2010**, *44*, 7783−7789.
(21) Riba, O.; Scott, T. B.; Ragnarsdottir, K. V.; Allen, G. C. *Geochim. Cosmochim. AC* **2008**, *72*, 4047−4057.
(22) Fiedor, J. N.; Bostick, W. D.; Jarabek, R. J.; Farrell, J. *Environ. Sci. Technol.* **1998**, *32*, 1466−1473.
(23) Ling, L.; Zhang, W. X. *Environ. Sci. Technol. Lett.* **2014**, *1*, 305−309.
(24) Ling, L.; Zhang, W. X. *Environ. Sci. Technol. Lett.* **2014**, *1*, 209−213.
(25) Scholl, J. A.; Koh, A. L.; Dionne, J. A. *Nature* **2012**, *483*, 421−427.
(26) Ilton, E. S.; Pacheco, J. S. L.; Bargar, J. R.; Shi, Z.; Liu, J.; Kovarik, L.; Engelhard, M. H.; Felmy, A. R. *Environ. Sci. Technol.* **2012**, *46*, 9428−9436.
(27) Cao, J. S.; Li, X. Q.; Tavakoli, J.; Zhang, W. X. *Environ. Sci. Technol.* **2008**, *42*, 3780−3785.
(28) Moore, K. T.; van der Laan, G. *Rev. Mod. Phys.* **2009**, *81*, 235−298.
(29) Moore, K. T.; van der Laan, G. *Ultramicroscopy* **2007**, *107*, 1201−1206.
(30) Chadwick, D.; Graham, J. *Nature* **1972**, *237*, 127−128.

DOI: 10.1021/ja510488r
J. Am. Chem. Soc. 2015, 137, 2788−2791